American Mineralogist, Volume 85, pages 1128–1142, 2000

Solubility behavior of water in haploandesitic melts at high pressure and high temperature

BJORN O. MYSEN[1,*] AND KEVIN WHEELER[2]

[1]Geophysical Laboratory and Center for High-Pressure Research (CHiPR), Carnegie Institution of Washington, 5251 Broad Branch Road, N.W., Washington D.C. 20015, U.S.A.
[2]Department of Geological Sciences, Brown University, Providence, Rhode Island 02912, U.S.A.

ABSTRACT

The solubility of H_2O in three melt compositions along the haploandesite join $Na_2Si_4O_9$-$Na_2(NaAl)_4O_9$ (0, 3, and 6 mol% Al_2O_3) was determined as a function of pressure and temperature from 0.8 to 2.0 GPa and 1000 to 1300 °C. Water solubility is a linear (or near-linear) positive function of pressure (16–18 mol% H_2O/GPa) at constant temperature, and a negative near-linear function of temperature (1–2 mol% H_2O/100 °C) at constant pressure. The solubility is correlated negatively with Al_2O_3 content of the melts.

Partial molar volume of H_2O in the melt, $\overline{V}_{H_2O}^{melt}$, was derived from solubility isotherms (1000, 1100, 1200, and 1300 °C) at 0.8, 1.05, 1.3, 1.65, and 2.0 GPa pressure. Values range between 7.8 and 12.8 cm^3/mol, and decrease with increasing Al_2O_3 content. In the pressure-temperature range studied, $(\partial \overline{V}_{H_2O}^{melt}/\partial T)_P$ ranges from -7.1 ± 0.810^{-3} to $-5.6 \pm 1.3 \cdot 10^{-3}$ cm^3/mol °C, becoming slightly less negative as the melts become more aluminous.

The $\overline{V}_{H_2O}^{melt}$ values were combined with published partial molar volume information for anhydrous oxides in silicate melts to estimate densities of water-rich dacitic magmas in shallow magma chambers associated with explosive volcanism. For a chamber of constant bulk composition during a comparatively short explosive event, such as that of Mount Pinatubo in June 1991 or Mount St. Helens in May 1980, the average density of the magma after eruption is ~3% higher than before the eruption occurred. Furthermore, because of removal of overburden during an eruption, the H_2O saturation value of remaining magma is less than that prior to eruption. From density calculations of the residual hydrous magma after eruption, its density decreases from top to bottom in the magma chamber. Consequently, this magma is gravitationally unstable.

INTRODUCTION

Characterization of the solubility and solubility behavior of H_2O in magmatic liquids is central to our understanding of igneous and hydrothermal processes, because dissolved H_2O governs most physicochemical properties of silicate melts. For example, the compositional trends of magmatic liquids during melting and crystallization are affected by water (e.g., Kushiro 1972, 1990; Mysen and Boettcher 1975; Gaetani et al. 1993), owing largely to reduction of silica activity in the magma. In addition, the viscosities of hydrous magmas are significantly lower than anhydrous magmas (Kushiro 1978; Schulze et al. 1996; Dingwell et al. 1998), and the densities of hydrous magmas deviate from their anhydrous equivalents (e.g., Kushiro 1978; see also Lange 1994, for a recent review). Therefore, the dynamics of magma aggregation, ascent, emplacement, and eruption depend on the water content of the magmatic liquid.

There is a substantial amount of data on water solubility and solubility behavior in magmatic liquids in the pressure regime of the Earth's crust (less than 1 GPa). Many igneous processes do, however, occur at higher pressure corresponding to those of the upper mantle. Water solubility data for magmatic systems at the pressure and temperature conditions in the upper mantle are much more scarce. These systems include those with melt compositions relevant to magmatic processes near convergent plate boundaries where magma-H_2O interactions are probably more important than in any other tectonic setting.

In this paper, we address some of these issues by providing H_2O solubility data for melts along the join $Na_2Si_4O_9$-$Na_2(NaAl)_4O_9$ as a function of temperature, pressure, and Al/(Al + Si). This join was chosen because the degree of melt polymerization (NBO/T = 0.5) is typical for that of andesitic magmatic liquids, and because alkalis are dominant network modifiers in such magmas (Mysen 1990). The data complement those of Mysen and Acton (1999), who examined the solubility behavior of H_2O in corresponding melt compositions in the system K_2O-Al_2O_3-SiO_2.

EXPERIMENTAL METHODS

Sample compositions were along the join $Na_2Si_4O_9$-$Na_2(NaAl)_4O_9$ with 0, 3, and 6 mol% Al_2O_3 added as $Na_2(NaAl)_4O_9$ (denoted NS4A3 and NS4A6). The Al-free composition is denoted NS4. Under the assumption that the Na-charge-balanced Al^{3+} is tetrahedrally coordinated in these melts, anhydrous melts retain their NBO/T-value of 0.5 as Al/(Al+Si) is increased. All compositions have Na/Al>1 and are, therefore, peralkaline.

Anhydrous starting glasses were made from mixtures of

*E-mail: mysen@gl.ciw.edu

0003-004X/00/0009–1128$05.00

spectroscopically pure Na_2CO_3, Al_2O_3, and SiO_2 ground under alcohol for about 1 h, decarbonated during slow heating (~1.5 °C/min), melted at 1250 °C at 0.1 MPa for 60 min, and then quenched to glass. Because of their hygroscopic nature, these glasses were stored at 400 °C when not in use. The analyzed compositions of the starting materials are given in Table 1.

High-pressure and high-temperature experiments were conducted in solid-media, high-pressure apparatus (Boyd and England 1960). The samples were contained in sealed Pt containers and subjected to experimental pressure and temperature conditions in 0.75"-diameter furnace assemblies based on the design of Kushiro (1976). Temperatures were measured with Pt-Pt90Rh10 thermocouples with no correction for pressure on their emf. Pressure was calibrated against the melting point of NaCl and the calcite-aragonite transformation. Estimated uncertainties are ± 10 °C and ± 0.1 GPa, respectively.

The starting glasses (10–15 mg of glass crushed to ~20 µm or less before use) were loaded together with double-distilled, deionized H_2O (1.0–2.5 µL depending on desired H_2O content) into 3 mm OD by 10 mm long Pt containers, and welded shut. The weighing accuracy is ± 0.02 mg. Water was injected using a microsyringe with 0.1 µL divisions. The exact amount of H_2O added was, however, determined by weighing. Reported H_2O contents of the experimental charges are accurate to ± 2% or better [2% for the lowest H_2O contents used (~5 wt% of the total sample)].

The quenched glasses (quenching rate >100 °C/s) in many of these samples contained clouds of finely distributed bubbles (typically <1 µm across) exsolved during quenching (Fig. 1). Similar bubbles were observed in the $K_2Si_4O_9$-$K_2(KAl)_4O_9$ glasses prepared by Mysen and Acton (1999). Therefore, analysis of the H_2O contents of the glasses by instrumental techniques was unreliable because it is not possible to account for H_2O lost by exsolution of H_2O from the melt during temperature-quenching to a hydrous glass.

To circumvent this problem, H_2O solubility in the melts was determined by locating the univariant phase boundary melt ↔ melt + vapor by examining the run products with a petrographic microscope (Burnham and Jahns 1962). The use of this method requires that bubbles in the glass formed by excess H_2O over that needed to saturate the melt at high pressure and temperature can be distinguished from those formed by H_2O exsolution from the melt during quenching. For the melt compositions examined here this distinction is quite straightforward as quench bubbles, when present, form clouds of small, often sub-micrometer bubbles. In contrast, bubbles formed by excess H_2O are typically ≥5 µm in diameter, and are distributed randomly in the quenched, hydrous glasses (Fig. 1). The uncertainty in H_2O solubility thus determined is taken as 1/2 that of each of the melt vs. melt+vapor brackets, and is less than 1 wt%. The reliability of this method was tested by using it to measure the H_2O solubility in $NaAlSi_3O_8$ melt at 1 GPa and 750 °C. The observed solubility at these conditions, 17.5 ± 0.5 wt% H_2O, compares well with the values of 17.2 wt% H_2O reported for 1 GPa and 690 °C by Burnham and Jahns (1962).

Run durations ranged from 300 min at the highest temperature (1300 °C) to 1440 min at the lowest temperature (1000 °C). Whether these run durations were sufficient to attain equilibrium can be evaluated by considering the diffusivity of H_2O in the melts. The diffusion constant, D, for H_2O in silicate melts such as those examined here (haploandesitic in composition) is likely to be somewhere between those of basaltic and rhyolitic melts at the same temperature and with the same H_2O contents. For those melts, the D-values range between ~10^{-8} and ~10^{-6} cm^2/s at temperatures near 1000 °C (e.g., Zhang and Stolper 1991; Nowak and Behrens 1997). From the simple relationship $x = \sqrt{4Dt}$ (x = diffusion distance, D = diffusion constant, and t = time) even a value for D as low as 10^{-8} cm^2/s would yield a transport distance for H_2O of ~ 270 µm after 300 min. With the ≤20 µm grain size of the starting material, the 300–1440 min run durations were, therefore, more than ad-

TABLE 1. Composition of glass starting material

	NS4	NS4A3	NS4A6
Na_2O	19.58	16.14	13.67
Al_2O_3	0.23	4.83	9.56
SiO_2	79.02	77.82	76.06
Total	98.83	98.80	99.30

Note: Analysis with JEOL 8900 superprobe using 15 kV accelerating voltage and 10 nA beam current, with the beam rastered over a 10 mm × 10 mm area. Because these high-alkali glasses are significantly volatile under the electron beam, the glasses were diluted with about 80 wt% $LiBO_2$, remelted, and vitrified prior to analysis.

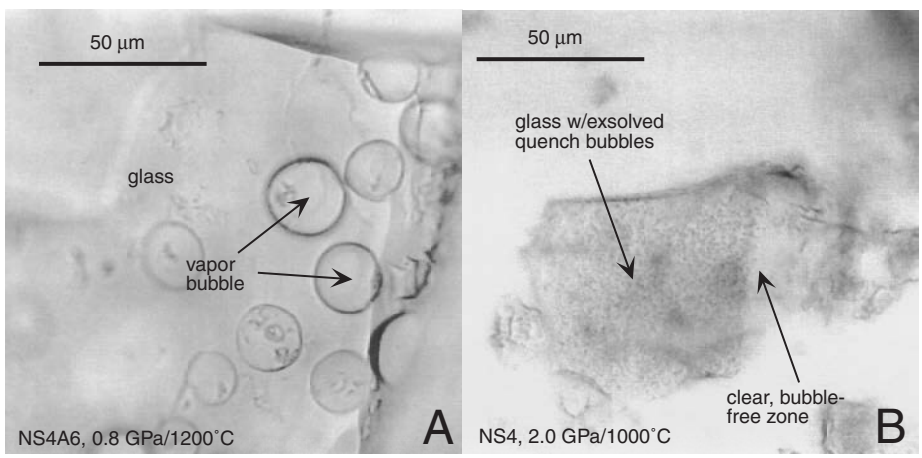

FIGURE 1. Photomicrographs of experimental charges illustrating the difference between vapor bubbles present stably during an experiment (**A**), and clouds of micrometer to submicrometer bubbles formed by exsolution of H_2O from cooling melt during quenching (**B**).

equate to ensure equilibrium during the experiments, provided that melt and aqueous fluid remained well mixed during experimentation. This was probably accomplished by convection within the 10 mm long by 3 mm diameter sample containers owing to the 10 °C vertical temperature gradient in the furnaces used (Kushiro 1976).

EXPERIMENTAL RESULTS

The experimental data are shown in Figures 2–4. The solid lines represent a third-order polynomial fit of the brackets to temperature at each pressure for each composition. The H_2O solubilities extracted from those fits are summarized in Table 2.

The solubility of H_2O in the Na_2Si_4-O_9-$Na_2(NaAl)_4O_9$ melts is a positive and linear (or near-linear) function of pressure (Fig. 5), a behavior similar to that of H_2O in haplogranitic melts (Holtz et al. 1995). For NS4 ($Na_2Si_4O_9$) and NS4A3 [$Na_2Si_4O_9$ + 3 mol% Al_2O_3 as $Na_2(NaAl)_4O_9$] composition melts, a straight line provides the best fit to the isothermal pressure-dependence of the solubility data (Table 3). For NS4A6 melt [$Na_2Si_4O_9$ + 6 mol% Al_2O_3 as $Na_2(NaAl)_4O_9$], the isothermal H_2O solubility is not quite a linear function of pressure. Instead, the pressure dependence, $(\partial \overline{V}_{H_2O}^{melt}/\partial P)_T$, increases with increasing pressure (Fig. 5; Table 3). For NS4, the pressure dependence may increase slightly with increasing temperature (from 17.8 ± 0.3 mol% H_2O/GPa at 1000 °C to 18.4 ± 0.7 mol% H_2O/GPa at 1300 °C), with an average value of 18.3 ± 0.5 mol%/GPa. The average pressure dependence for NS4A3 melt is 16.2 ± 0.2 mol% H_2O/GPa. These values compare well with the pressure dependence of H_2O solubility in corresponding K_2O-Al_2O_3-SiO_2 melts (16.8 ± 1.5 and 18.7 ± 0.5 mol% H_2O/GPa for compositions KS4 and KS4A3, respectively; Mysen and Acton 1999).

The relationship between temperature and H_2O solubility is shown in Figure 5. The data for corresponding melt compositions in the system K_2O-Al_2O_3-SiO_2 (Mysen and Acton 1999) are shown for comparison. For both systems, the water solubility decreases linearly with increasing temperature at constant pressure at a rate of 1–2 mol% H_2O/100 °C (Table 4). There is no evidence for a transition from retrograde to prograde solubility in the 0.8–2.0 GPa pressure range. This result contrasts with water solubility data for albitic and haplogranitic melts obtained at pressures near 0.5 GPa (Paillat et al. 1992; Holtz et al. 1995). For those melt compositions below that pressure, water solubility decreases with increasing temperature (retrograde solubility). At higher pressure, water solubility increases with increasing temperature (prograde solubility). The latter melt compositions are both more aluminous and considerably more polymerized than those under consideration here, which may account for the difference in temperature-dependent solubility behavior.

Shen and Keppler (1997), using a hydrothermal diamond-anvil cell for in-situ examination of melt behavior, observed complete miscibility between $NaAlSi_3O_8$ melt and H_2O at $P \geq$ 10 GPa and $T \geq$ 1000 °C. Bureau and Keppler (1999) performed similar experiments with $NaAlSi_2O_6$, $NaAlSiO_4$, and haplogranitic melts. These three compositions exhibited

TABLE 2. Solubility of H_2O in melts (mol%, based on O = 1)

T, °C	NS4	NS4A3	NS4A6
	0.8 GPa		
1000	17.8 ± 2.3	12.2 ± 0.3	10.5 ± 1.2
1100	16.4 ± 3.0	11.7 ± 0.4	9.4 ± 0.7
1200	14.6 ± 0.8	11.2 ± 0.7	8.7 ± 0.3
1300	12.3 ± 0.9	9.0 ± 0.4	7.8 ± 0.4
	1.05 GPa		
1000	21.3 ± 0.8	17.3 ± 0.9	14.5 ± 0.7
1100	20.1 ± 0.4	15.7 ± 0.4	13.2 ± 0.4
1200	18.7 ± 0.5	14.1 ± 0.9	11.8 ± 1.7
1300	17.5 ± 0.4	12.2 ± 0.9	10.5 ± 0.9
	1.3 GPa		
1000	26.2 ± 0.3	21.1 ± 0.6	17.8 ± 0.4
1100	24.8 ± 0.7	18.5 ± 0.6	17.0 ± 0.4
1200	23.3 ± 2.2	17.3 ± 0.3	15.7 ± 0.4
1300	20.7 ± 1.6	15.4 ± 0.3	13.8 ± 0.7
	1.65 GPa		
1000	32.7 ± 1.9	26.1 ± 1.4	25.1 ± 0.8
1100	32.5 ± 0.2	25.3 ± 0.8	23.9 ± 0.3
1200	30.6 ± 0.4	24.5 ± 0.7	21.7 ± 1.2
1300	28.5 ± 0.8	23.1 ± 1.6	19.8 ± 1.0
	2.0 GPa		
1000	38.6 ± 1.5	32.2 ± 1.4	32.2 ± 0.5
1100	37.1 ± 0.8	31.1 ± 0.7	31.3 ± 0.8
1200	36.8 ± 1.1	29.8 ± 0.4	29.3 ± 0.6
1300	34.5 ± 1.3	28.0 ± 0.4	26.7 ± 0.5

TABLE 3. Pressure dependence of H_2O solubility (mol H_2O = a + bP + cP^2)

T, °C	a	b	c	R^2
	0% Al_2O_3 (NS4)			
1000	3.0 ± 0.3	17.9 ± 0.3	–	0.999
1100	1.8 ± 1.2	17.9 ± 0.8	–	0.996
1200	–0.7 ± 0.6	18.8 ± 0.4	–	0.999
1300	–2.4 ± 0.9	18.5 ± 0.7	–	0.998
	3% Al_2O_3 (NS4A3)			
1000	–0.3 ± 0.8	16.2 ± 0.5	–	0.998
1100	–1.6 ± 0.9	16.2 ± 0.7	–	0.998
1200	–2.3 ± 1.4	16.0 ± 0.9	–	0.996
1300	–4.7 ± 1.3	16.4 ± 0.9	–	0.995
	6% Al_2O_3 (NS4A6)			
1000	2.4 ± 2.6	7.1 ± 3.0	3.9 ± 1.4	0.999
1100	1.0 ± 1.1	7.4 ± 1.7	3.9 ± 0.6	1.000
1200	2.6 ± 0.8	3.8 ± 1.1	4.8 ± 0.4	1.000
1300	3.4 ± 0.5	1.4 ± 0.8	5.1 ± 0.3	1.000

TABLE 4. Temperature dependence of H_2O solubility (mol% H_2O = a + bT)

P, GPa	a	b	R^2
	0% Al_2O_3 (NS4)		
0.8	36.3 ± 1.6	–0.018 ± 0.001	0.988
1.05	34.3 ± 0.3	–0.0130 ± 0.0002	0.999
1.3	44.4 ± 2.2	–0.018 ± 0.002	0.978
1.65	48.0 ± 3.5	–0.015 ± 0.003	0.920
2.0	51.2 ± 3.1	–0.013 ± 0.003	0.916
	3% Al_2O_3 (NS4A3)		
0.8	22.5 ± 3.4	–0.010 ± 0.003	0.854
1.05	34.3 ± 0.7	–0.0170 ± 0.0006	0.998
1.3	39.2 ± 2.1	–0.018 ± 0.002	0.982
1.65	36.1 ± 1.3	–0.010 ± 0.001	0.974
2.0	46.5 ± 1.3	–0.014 ± 0.001	0.986
	6% Al_2O_3 (NS4A5)		
0.8	21.9 ± 0.2	–0.0114 ± 0.0001	1.000
1.05	22.3 ± 0.7	–0.0092 ± 0.0006	0.992
1.3	31.9 ± 1.9	–0.014 ± 0.002	0.972
1.65	43.6 ± 1.8	–0.018 ± 0.002	0.986
2.9	44.9 ± 0.9	–0.0126 ± 0.0008	0.992

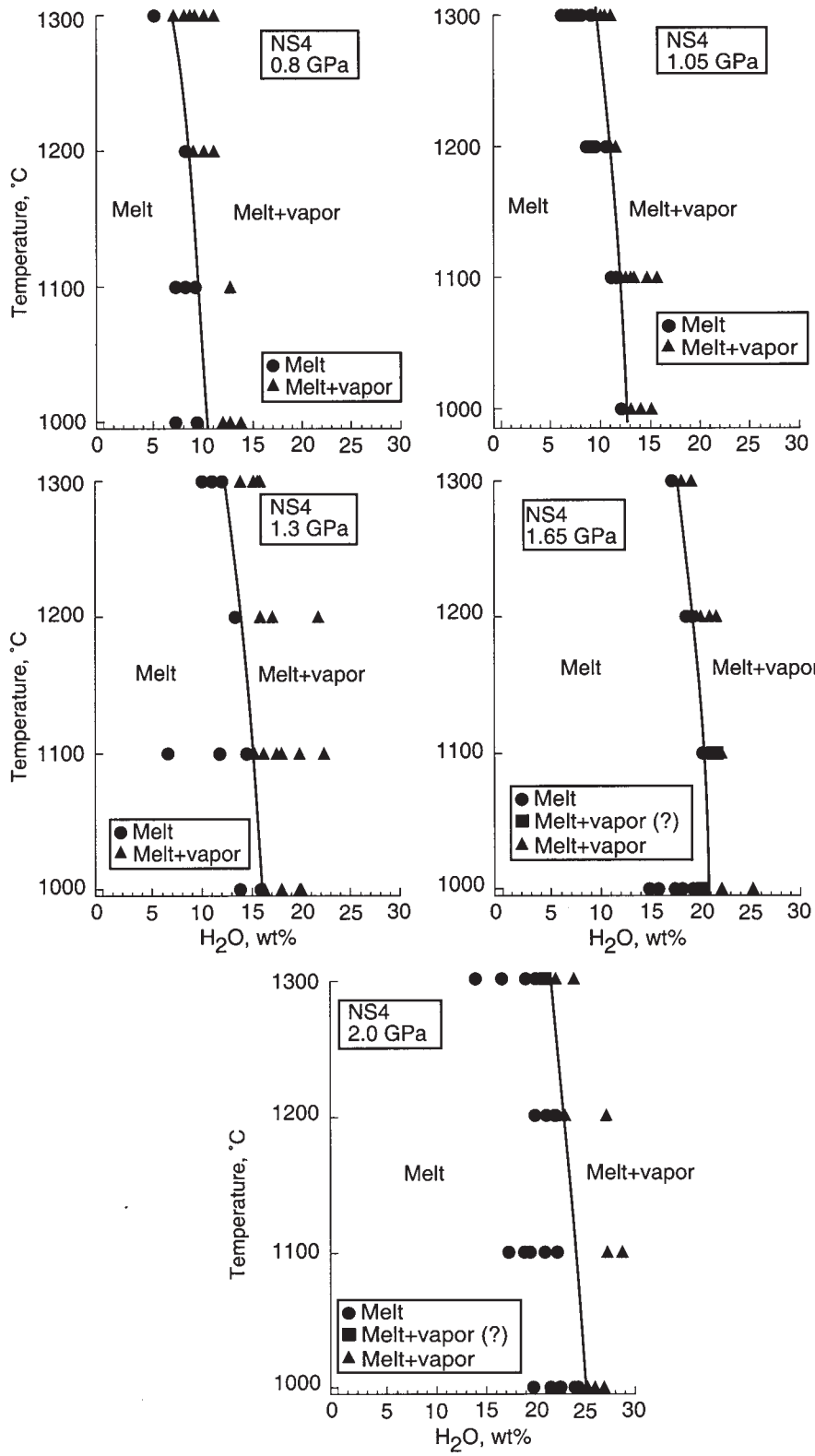

FIGURE 2. Experimental results for composition NS4 ($Na_2Si_4O_9$) at the pressures indicated. Symbols are defined within the individual panels. Filled squares denote cases where identification of "large" vapor bubbles that indicate the presence of excess H_2O during an experiment could not be established with certainty. The solid lines represent a third-order polynomial fit of the brackets to temperature at each pressure for each composition.

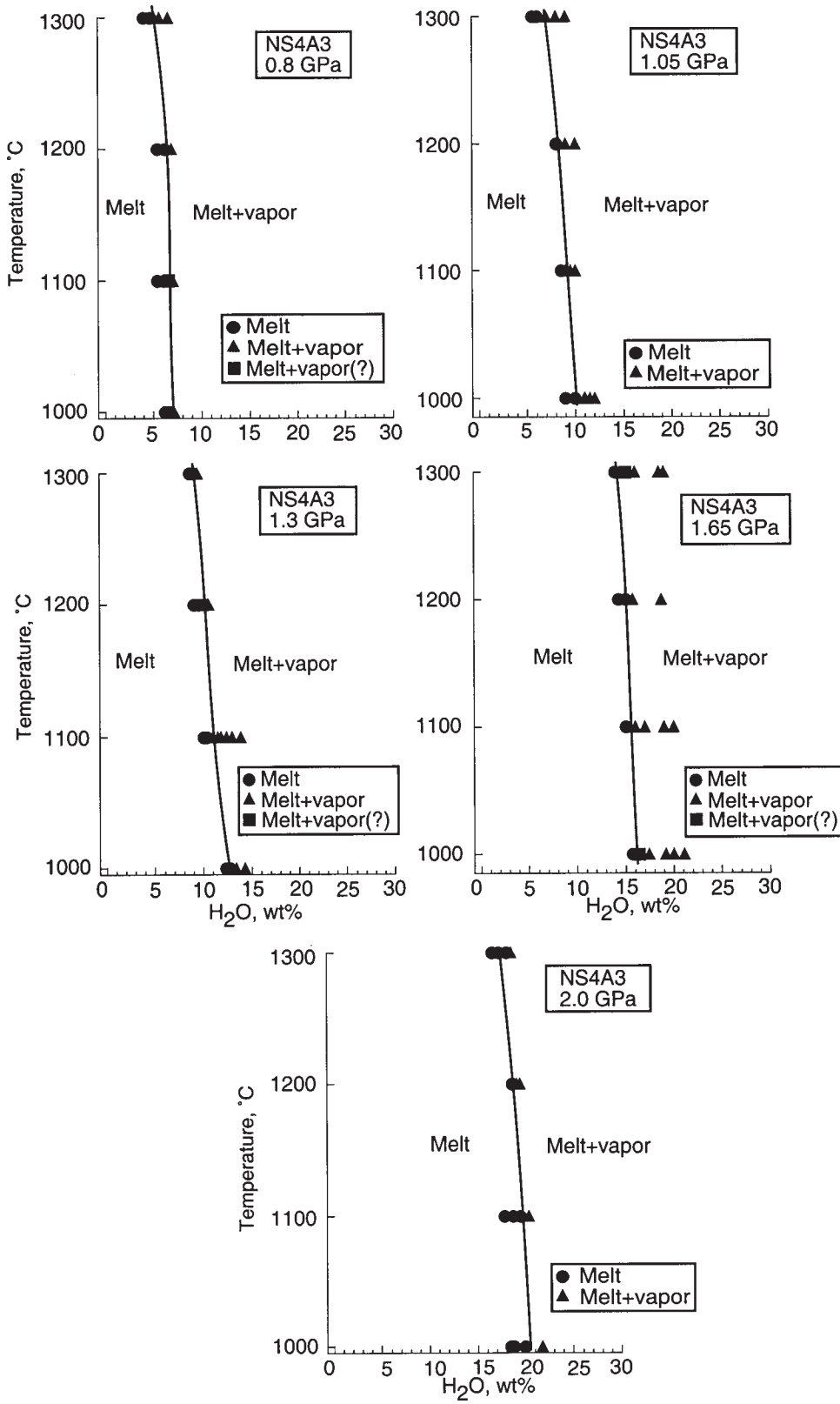

FIGURE 3. Same as Figure 2, but for composition NS4A3 [$Na_2Si_4O_9$ + 3 mol% Al_2O_3 added as $Na_2(NaAl)_4O_9$ component].

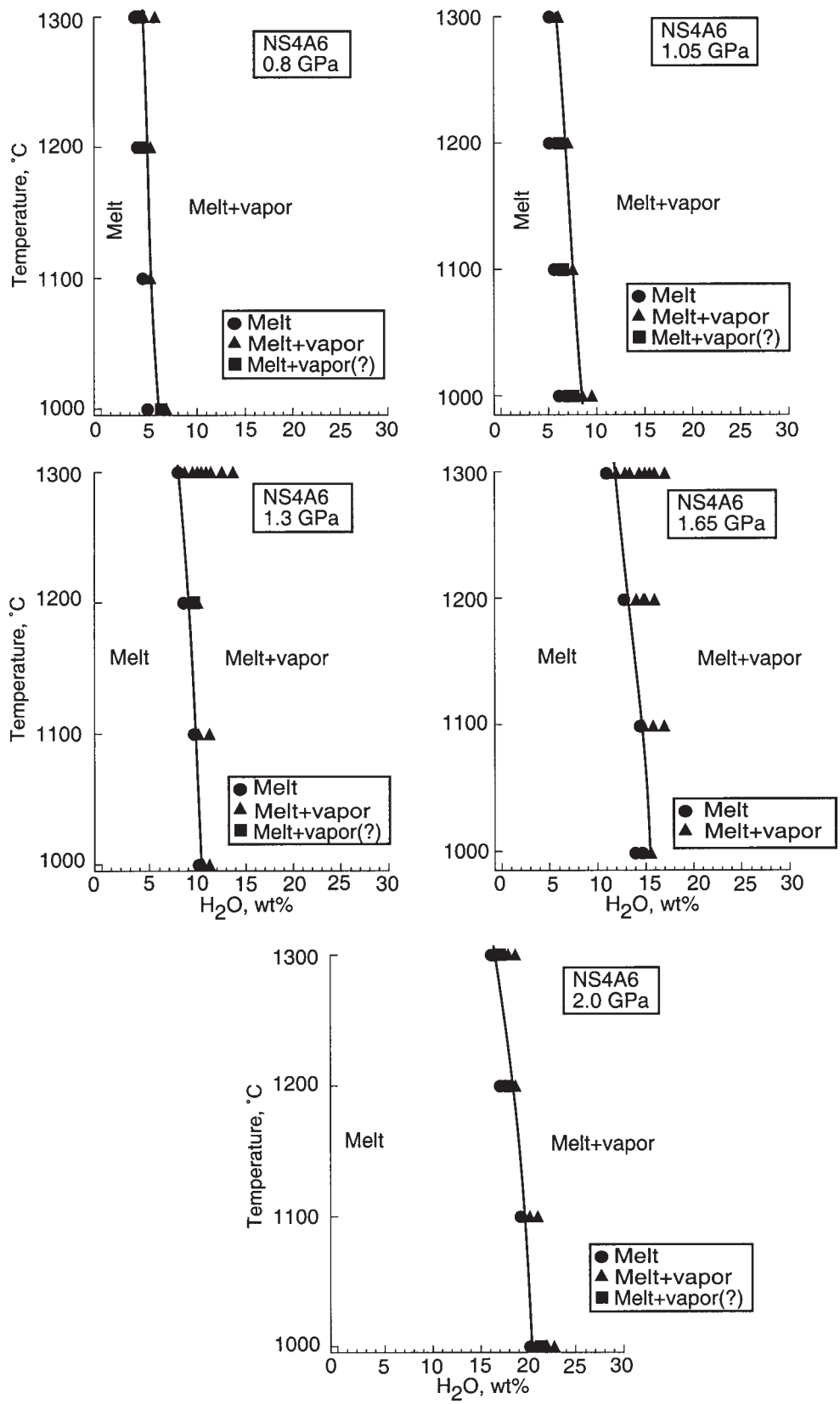

FIGURE 4. Same as Figure 2, but for composition NS4A6 [$Na_2Si_4O_9$ + 6 mol% Al_2O_3 added as $Na_2(NaAl)_4O_9$ component].

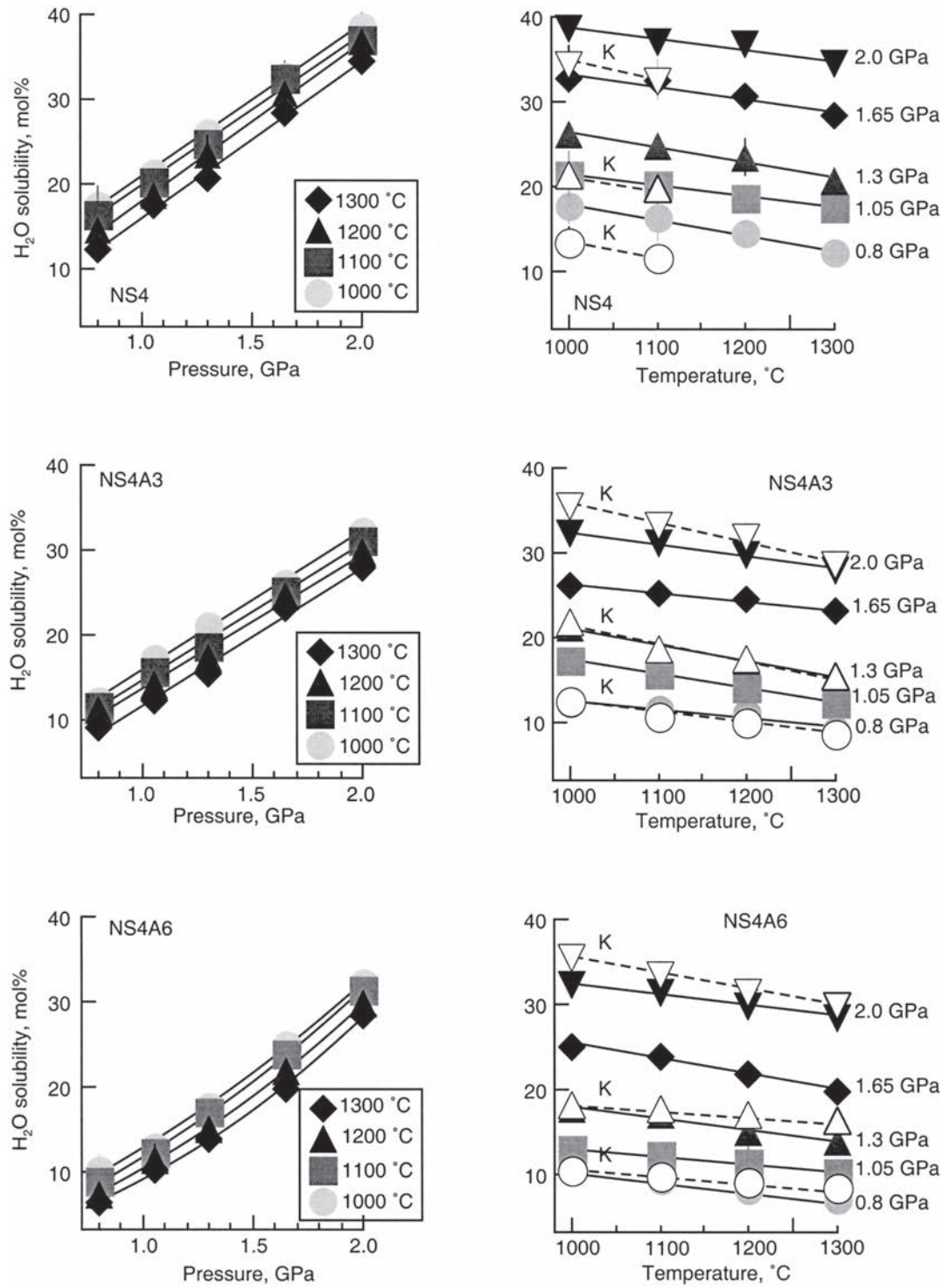

FIGURE 5. Solubility of H_2O in the indicated melt compositions as a function of temperature and pressure. The solubility was calculated on the basis of O 1. Filled symbols = melts on the join Na_2Si_4-O_9-$Na_2(NaAl)_4O_9$; open symbols = melts on the join K_2Si_4-O_9-$K_2(KAl)_4O_9$ (data from Mysen and Acton 1999). When not shown, error bars are smaller than the symbol size.

supercritical behavior at $P \geq 1$ GPa and $T \geq 1000$ °C. These observations contrast with the behavior of H_2O dissolved in NS4, NS4A3, and NS4A6 melts, where there is no evidence that the systems approach supercriticality because the temperature dependence of the solubility of H_2O in the melts, $(\partial \overline{V}_{H_2O}^{melt}/\partial T)_P$, is negative at all pressures.

There are two possible reasons for this difference. First, the melts studied by Shen and Keppler (1997) and Bureau and Keppler (1999) are considerably more aluminous and more polymerized than those examined in the present study. Second, pressure estimates in the hydrothermal diamond-anvil cell are obtained by using the *P-V-T* properties of pure H_2O (temperature is measured by a thermocouple and the sample volume in the cell is essentially constant). An aqueous solution in equilibrium with alkali aluminosilicate melts at $P \geq 1$ GPa and high temperature is not pure H_2O, but rather is quite rich in silicate materials (perhaps exceeding 10–20 wt%, Mysen and Acton 1999; Stalder et al. 2000). The solubility varies with both temperature and pressure. The *P-V-T* properties of such silicate-saturated aqueous fluids, required for precise pressure calculations, are not known, but are probably significantly different from those of pure H_2O. Thus, the pressure in the hydrothermal diamond anvil cell in the pressure and temperature range under consideration is not well known. It is suggested, therefore, that the different water solubility behavior reported in this paper compared with those of Shen and Keppler (1997) and Bureau and Keppler (1999) could be due to a combination of the different bulk chemical compositions of the melts, and to an inability to measure pressure precisely in the diamond-anvil studies.

Increasing Al_2O_3 also results in lower H_2O solubility (Fig. 6), similar to other aluminosilicate melts (Dingwell et al. 1997). The effect of Al_2O_3 appears to be more pronounced for melts along the join $Na_2Si_4O_9$-$Na_2(NaAl)_4O_9$ than for those along the $K_2Si_4O_9$-$K_2(KAl)_4O_9$ join (Mysen and Acton 1999). The relationship between H_2O solubility and Al_2O_3 becomes distinctly more non-linear with increasing pressure.

Discussion

Partial molar volume of H_2O in melts

The H_2O solubility data presented in Tables 2–4 can be used to calculate partial molar volumes of H_2O in the melts. For H_2O-saturated silicate melt in equilibrium with free H_2O, the Gibbs free energy of solution of H_2O is (in J/mol):

$$\Delta G_T(P) = 0 = \Delta G_T(1\text{bar}) + RT \ln \frac{a_{H_2O}^{melt}}{f_{H_2O}^{o}} + \int_1^P \overline{V}_{H_2O}^{melt} dP \quad (1)$$

where R is the universal gas constant (82.157 cm^3·bar/mol K), T is temperature (Kelvin) $a_{H_2O}^{melt}$ is the activity of H_2O in the melt, $f_{H_2O}^{o}$ is the fugacity of pure H_2O in bars, and $\overline{V}_{H_2O}^{melt}$ (cm^3/mol) is the partial molar volume of H_2O in the melt (e.g., Hodges 1974). The activity of H_2O, $a_{H_2O}^{melt}$, is not known. We assume, therefore, that the mol fraction, $X_{H_2O}^{melt}$, may be substituted for $a_{H_2O}^{melt}$. Calorimetric data for $NaAlSi_3O_8$-H_2O glasses indicate only a small negative heat of mixing (0–49 kJ/mol) (Clemens and Navrotsky 1987). The assumption $a_{H_2O}^{melt} = X_{H_2O}^{melt}$ would not, therefore, introduce a large error in these calculations.

The slope of the $(P-1)/RT$ vs. $\ln(f_{H_2O}^{0}/X_{H_2O}^{melt})$ equals $\overline{V}_{H_2O}^{melt}$ at given temperature, T (e.g., Lange 1994). In the 0.8–2.0 GPa pressure range examined here, these lines are straight (Fig. 7), a result that is consistent with the assumption that the mol fraction of H_2O in the melt, $X_{H_2O}^{melt}$, can be replaced with its activity, $a_{H_2O}^{melt}$, in Equation 1.

The straight lines in Figure 7 also imply that the partial molar volume of H_2O, $\overline{V}_{H_2O}^{melt}$, does not vary with pressure in this pressure range within the uncertainty of the calculated partial molar volume values. The uncertainty in $\overline{V}_{H_2O}^{melt}$ reflects the progression of the errors in the measured water solubilities for the melts. $\overline{V}_{H_2O}^{melt}$ ranges between ~8 and ~12 cm^3/mol (Fig. 8) and decreases with increasing Al_2O_3 and with increasing temperature. The latter two effects were also noted for H_2O dissolved in corresponding KS4, KS4A3, and KS4A6 melts in the same pressure range (Mysen and Acton 1999). The $\overline{V}_{H_2O}^{melt}$ in the potassic melts is, however, consistently lower (by 7–11%), and $(\partial \overline{V}_{H_2O}^{melt}/\partial T)_P$ is less negative than for corresponding melts in the Na_2O-Al_2O_3-SiO_2 system (Fig. 8).

The $\overline{V}_{H_2O}^{melt}$ values in Figure 8 compare reasonably well with those calculated from water solubility data for haplogranite ($Qz_{28}Ab_{38}Or_{34}$), albite and diopside composition melts (Holtz et al. 1995; Burnham and Davis 1971; Paillat et al. 1992; Hodges 1974), and for andesite glass (Richet and Polian 1998). The H_2O solubility data of Holtz et al. (1995) for $Qz_{28}Ab_{38}Or_{34}$ melt between 0.03 and 0.8 GPa at 800 °C, yield values for $\overline{V}_{H_2O}^{melt}$ that decrease exponentially from ~32 cm^3/mol at 0.03 GPa to about 12.5 cm^3/mol at 0.5 GPa. The 1400 °C water solubility isotherm for $NaAlSi_3O_8$ melt (Paillat et al. 1992) results in $\overline{V}_{H_2O}^{melt}$ decreasing as a non-linear function of pressure from ~ 41 to ~ 12 cm^3/mol between 0.2 and 0.4 GPa (average $\partial \overline{V}_{H_2O}^{melt}/\partial P = -14.5 \cdot 10^{-3}$ cm^3/mol·bar). Those results, extrapolated to 1–2 GPa, indicate that $\overline{V}_{H_2O}^{melt}$ for $NaAlSi_3O_8$ melt is in the 11–14 cm^3/mol range, thus not differing greatly from the $\overline{V}_{H_2O}^{melt}$ of the present study.[1] The $\overline{V}_{H_2O}^{melt}$ data in Figure 8, as well as those derived from literature solubility data, are somewhat lower than those deduced from thermal expansion and compressibility data for $NaAlSi_3O_8$-H_2O glass and melt by Ochs and Lange (1997) (17–20 cm^3/mol). This difference may result from their assumption that $(\partial \overline{V}_{H_2O}^{melt}/\partial T)_P$ and $(\partial \overline{V}_{H_2O}^{melt}/\partial P)_T$ are constants. That assumption is not supported by the pressure- and temperature-derivatives of $\overline{V}_{H_2O}^{melt}$ extracted from water solubility data or by the direct volume measurements reported by Burnham and Davis (1971). In the latter cases, the $(\partial \overline{V}_{H_2O}^{melt}/\partial P)_T$ is distinctly non-linear, particularly at the lower pressures. This non-linearity may reflect a significant compressibility of the fraction of water dissolved in molecular form in the melt. If so, because the proportion of water dissolved in molecular form increases with increasing total water content (e.g., Stolper 1982), it would be expected that $(\partial \overline{V}_{H_2O}^{melt}/\partial P)_T$ would decrease with decreasing water content of silicate melts.

The negative correlation between $\overline{V}_{H_2O}^{melt}$ and Al_2O_3 content may be attributable to the solution mechanism of H_2O in alu-

[1] The $(\partial \overline{V}_{H_2O}^{melt}/\partial P)_T$ for all these melts diminishes rapidly with increasing pressure. At 0.5 GPa, for example, the $(\partial \overline{V}_{H_2O}^{melt}/\partial P)_T$ is $\leq -1 \cdot 10^{-3}$ cm^3/mol bar.

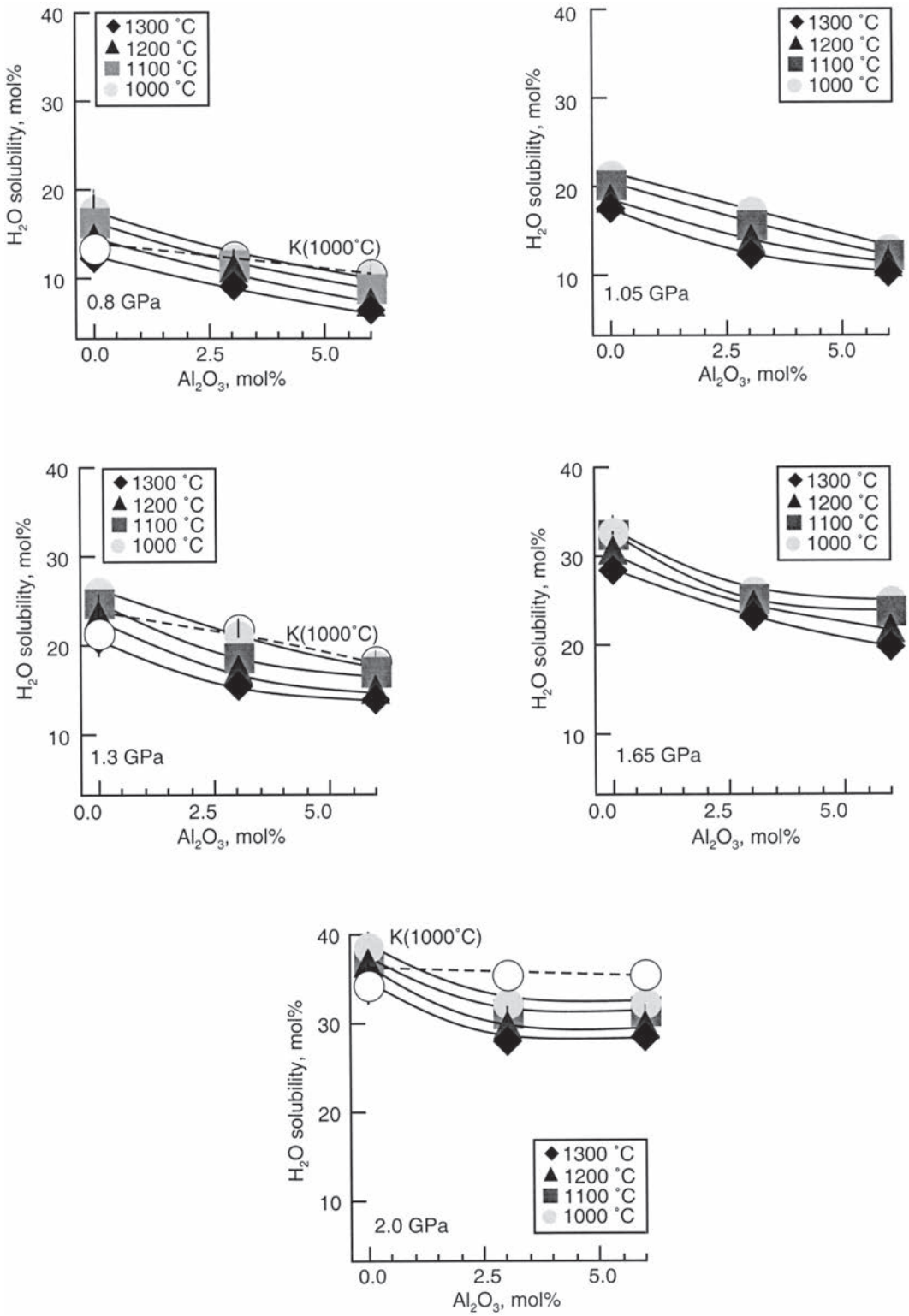

FIGURE 6. Solubility of H_2O in the indicated melt compositions as a function of Al_2O_3 content at the indicated pressures and temperatures. Solubilities were calculated on the basis of O = 1. Filled symbols = melts on the join $Na_2Si_4O_9$-$Na_2(NaAl)_4O_9$; open symbols = melts on the join $K_2Si_4O_9$-$K_2(KAl)_4O_9$ (data from Mysen and Acton 1999). Error bars when not shown are smaller than the symbol size.

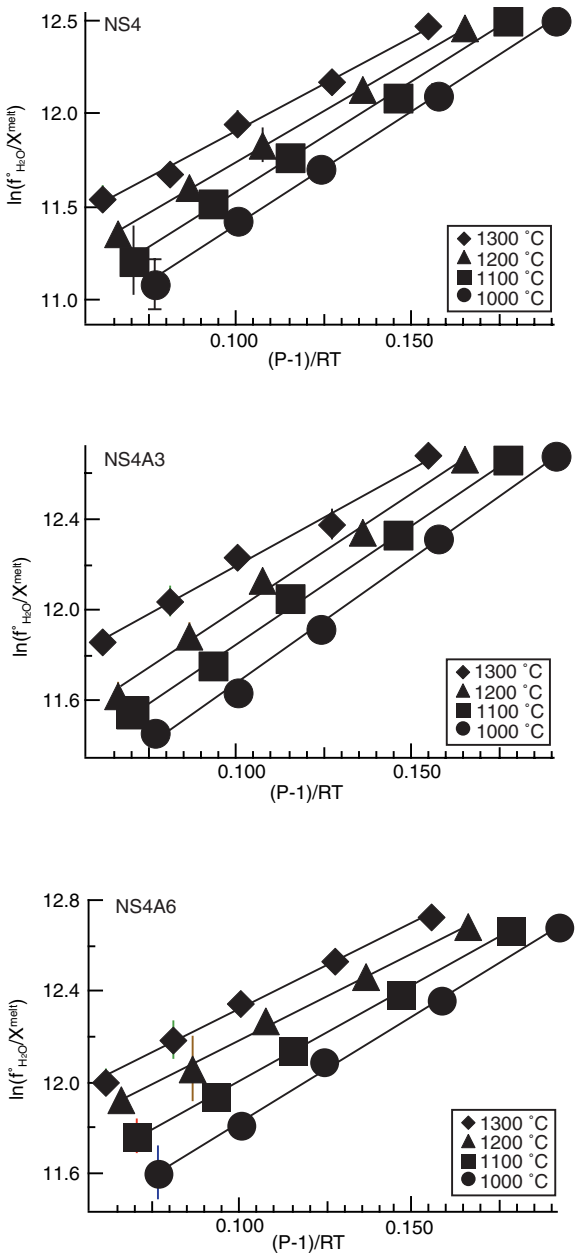

FIGURE 7. A plot of ln ($f^0_{H_2O}/X^{melt}_{H_2O}$) vs. ($P$–1)/R$T$, where $f^0_{H_2O}$ is the fugacity of H_2O obtained from the model of Haar et al. (1984), $X^{melt}_{H_2O}$ is the mol fraction of H_2O in the melts, P is the pressure (bar), R is the gas constant, and T is the temperature (K). When error bars are not shown, the errors are smaller than the size of the symbols.

minosilicate melts, which differs from the mechanism in Al-free silicate melts (Mysen and Virgo 1986). In Al-free alkali silicate melts, H_2O interacts with the melt components to form Si···OH and alkali···OH complexes. In alkali aluminosilicate melts, on the other hand, Al···OH and alkali···OH complexing is likely. There is no evidence for Si···OH bonding in such melts (Mysen and Virgo 1986; Kohn et al. 1992).

Perhaps one of the most surprising aspects of the partial molar volume results in Figure 8 is the negative $(\partial \overline{V}^{melt}_{H_2O}/\partial T)_P$ (–7.1 ± 0.8·10^{-3} to –5.2 ± 1.3·10^{-3} cm^3/mol °C depending on melt composition). The $(\partial \overline{V}^{melt}_{H_2O}/\partial T)_P$ determined at lower pressure (Burnham and Davis 1971), and $(\partial \overline{V}^{melt}_{H_2O}/\partial T)_P$ derived from water solubility data for $NaAlSi_3O_8$ and $Qz_{28}Ab_{38}Or_{34}$ melts at pressures <0.2–0.3 GPa (Holtz et al. 1995; Paillat et al. 1992; Hamilton and Oxtoby 1986), indicate that $(\partial \overline{V}^{melt}_{H_2O}/\partial T)_P$ is positive. However, at pressures above ~0.2 GPa, $(\partial \overline{V}^{melt}_{H_2O}/\partial T)_P$ derived from water solubility data for the $Qz_{28}Ab_{38}Or_{34}$ melt composition (Holtz et al. 1995) changes sign from positive to negative (Fig. 9). For the $NaAlSi_3O_8$ melt composition the calculated $(\partial \overline{V}^{melt}_{H_2O}/\partial T)_P$ between 900 and 1100 °C decreases with increasing pressure and is near 0 or slightly negative at $P \geq 0.5$ GPa. The negative $(\partial \overline{V}^{melt}_{H_2O}/\partial T)_P$ values for the melt compositions investigated in the present study (and also those of the analogous potassium system; see Fig. 8), obtained at $P \geq 0.8$ GPa, are consistent with the higher-pressure $(\partial \overline{V}^{melt}_{H_2O}/\partial T)_P$ trends exhibited by the $Qz_{28}Ab_{38}Or_{34}$ and $NaAlSi_3O_8$ melts.

The pressure-induced changes in $(\partial \overline{V}^{melt}_{H_2O}/\partial T)_P$ from positive to negative may be related to pressure- and temperature-dependent speciation in the melts (i.e., water in molecular form, H_2O, and as OH groups). For pure H_2O, the $\partial V^0_{H_2O}/\partial T$ ($V^0_{H_2O}$ = molar volume of pure H_2O) is always positive, but decreases with increasing pressure (e.g., Haar et al. 1984; Brodholt and Wood 1993; see also Fig. 9). It is unlikely, therefore, that the temperature-derivative of the partial molar volume of water as molecular H_2O could become negative with increasing pressure. Instead, we suggest that the change in the sign of $(\partial \overline{V}^{melt}_{H_2O}/\partial T)_P$ with increasing pressure is related to the partial molar volume of H_2O of the portion of water dissolved as OH.

For the simple speciation reaction for H_2O in melts:

$$H_2O + O^{2-} \leftrightarrow 2OH^-. \qquad (2)$$

ΔH is approximately 30 kJ/mol (Nowak and Behrens 1995; Shen and Keppler 1995; Withers et al. 1999). In other words, OH/(OH+H_2O) increases with increasing temperature. Provided that $\overline{V}^{melt}_{H_2O}$ (OH) < $\overline{V}^{melt}_{H_2O}$ < $\overline{V}^{melt}_{H_2O}$ (H_2O) and $[\partial \overline{V}^{melt}_{H_2O}$ (H_2O)/$\partial T]_P$ decreases with increasing pressure, the value for bulk water in the melt, $(\partial \overline{V}^{melt}_{H_2O}/\partial T)_P$, might change sign from positive to negative with increasing pressure.

Alternatively, the change of $(\partial \overline{V}^{melt}_{H_2O}/\partial T)_P$ from positive at low pressure to negative at high pressure might be related to the assumption that $a^{melt}_{H_2O} = X^{melt}_{H_2O}$ in Equation 1. If so, the implication is that at low pressure [where $(\partial \overline{V}^{melt}_{H_2O}/\partial T)_P > 0$], $a^{melt}_{H_2O}$ decreases with increasing temperature, whereas at higher pressure [where $(\partial \overline{V}^{melt}_{H_2O}/\partial T)_P < 0$], $a^{melt}_{H_2O}$ increases with increasing temperature. To our knowledge, no thermodynamic data exist that are consistent with such a highly unusual behavior of H_2O in water-saturated aluminosilicate melts. This alternative is, therefore, considered highly unlikely.

Applications

Density of anhydrous vs. hydrous melts. The density of anhydrous and water-saturated NS4, NS4A3, and NS4A6 composition melts was calculated with the $\overline{V}^{melt}_{H_2O}$ and H_2O solubility data from the present study coupled with thermal expansion and compressibility data of anhydrous oxide components

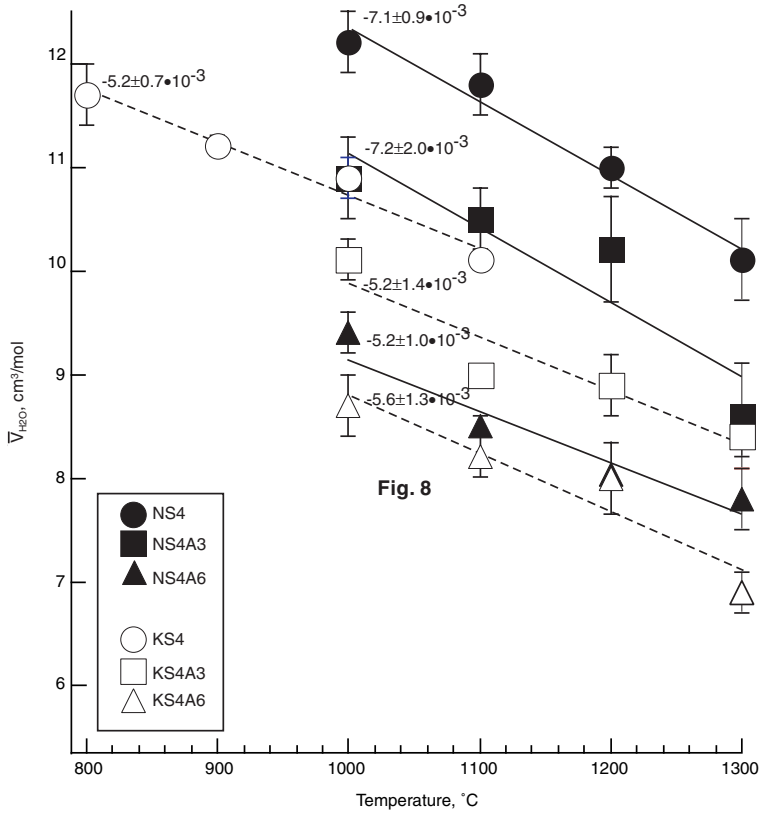

FIGURE 8. Partial molar volume of H_2O, $\overline{V}_{H_2O}^{melt}$, for the indicated melt compositions as a function of temperature. The numbers on individual straight line fits are values for $\partial \overline{V}_{H_2O}^{melt} / \partial T$ (cm³/mol·°C). Filled symbols = melts on the join $Na_2Si_4O_9$-$Na_2(NaAl)_4O_9$; open symbols = melts on the join $K_2Si_4O_9$-$K_2(KAl)_4O_9$ (H_2O solubility data from Mysen and Acton 1999).

(Lange and Carmichael 1987; Kress and Carmichael 1991). The calculations were performed for 1000 °C in the 0.8–2.0 GPa pressure range (Fig. 10). Also shown (open symbols) are the densities of corresponding K-melts (KS4, KS4A3, and KS4A6) from Mysen and Acton (1999).

By saturating the melts on the $Na_2Si_4O_9$-$Na_2(NaAl)_4O_9$ join with H_2O, the melt density decreases by nearly 23% for the Al-free $Na_2Si_4O_9$ (NS4) composition at 2.0 GPa. This density decrease diminishes with increasing Al_2O_3 content so that for composition NS4A6, the H_2O-saturated melt at 2.0 GPa is about 10% less dense than its anhydrous equivalent (Fig. 10). The dominating influence of H_2O on the melt density is the partial molar volume of H_2O, which decreases with increasing Al_2O_3 (the H_2O solubility is not very sensitive to Al_2O_3 content, see Fig. 5). As a result, the more aluminous the melt, the less of a density difference between anhydrous and H_2O-saturated melts.

The density difference between hydrous and anhydrous melts decreases with decreasing pressure for all compositions. This pressure effect is, of course, because the results in Figure 10 are for water-saturated melts. The H_2O solubility of the melts increases with increasing pressure. At constant total water content, as illustrated by density difference calculations with 5 wt% H_2O (Fig. 10B), the pressure effect on the density difference is essentially removed. The remaining slight positive correlation of the density difference with pressure is the result of the constant partial molar volume of H_2O in the range 0.8–2.0 GPa, whereas the pressure derivatives of the oxide volumes are

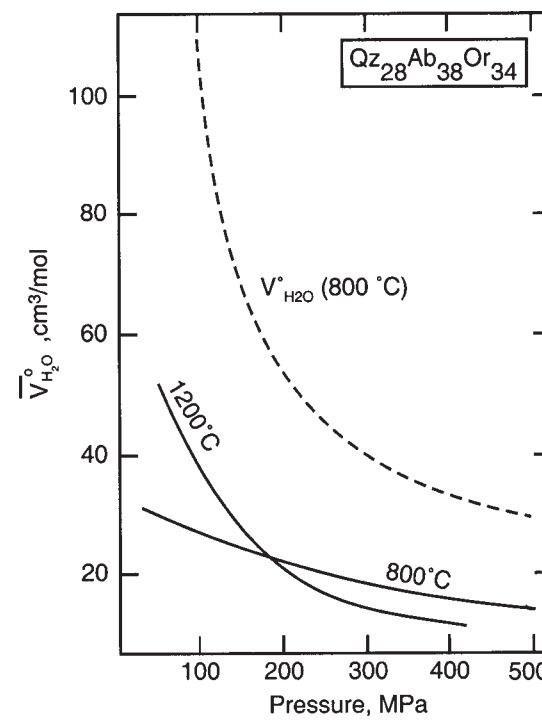

FIGURE 9. Calculated partial molar volume of H_2O, $\overline{V}_{H_2O}^{melt}$, from H_2O solubility data for composition $Qz_{28}Ab_{38}Or_{34}$ (20 mol% SiO_2, 38 mol% $NaAlSi_3O_9$, 34 mol% $KAlSi_3O_8$) at 800 and 1200 °C as a function of pressure (solubility data from Holtz et al. 1995). Also shown is the molar volume of H_2O, $V_{H_2O}^0$, at 800 °C as a function of pressure (calculated from the equation of state developed by Haar et al. 1984).

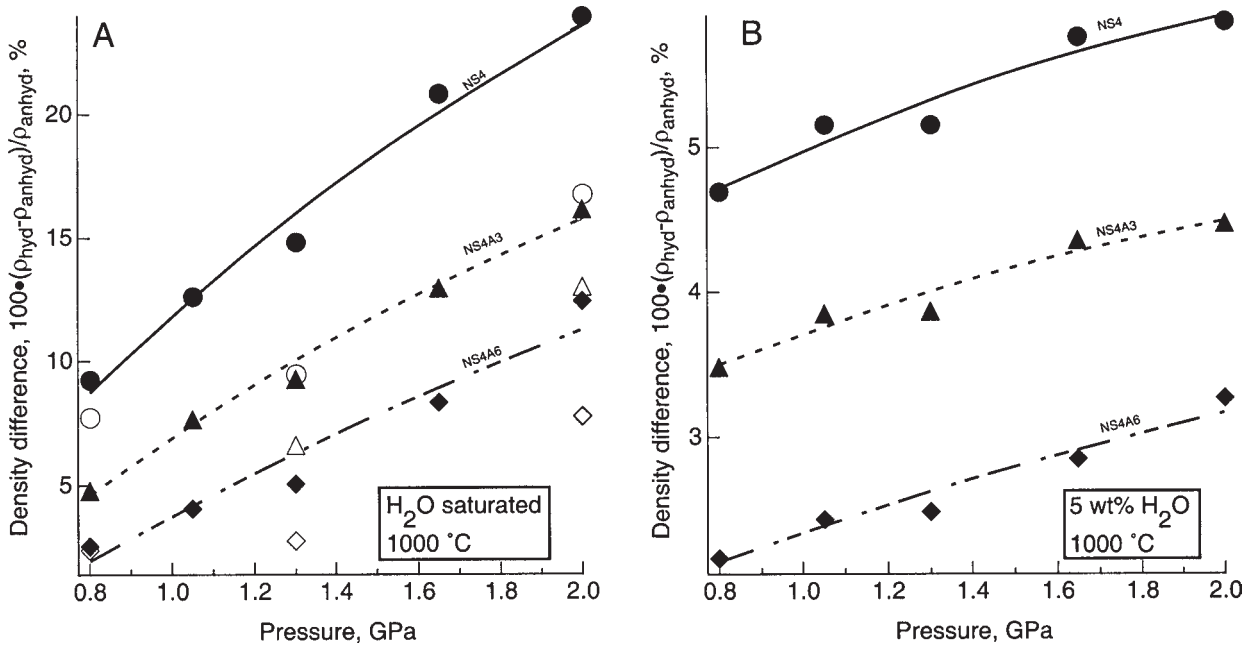

FIGURE 10. Density difference between hydrous, ρ_{hyd}, and anhydrous, ρ_{anhyd}, melts relative to that of anhydrous melt as a function of pressure at 1000 °C. (**A**) calculated for water-saturated melts at 0.8–2.0 GPa. (**B**) Calculated for melts containing 5 wt% H_2O. Partial molar volume, thermal expansion, and compressibility data for anhydrous components, Na_2O, Al_2O_3, and SiO_2, were obtained from Lange and Carmichael (1987) and Kress and Carmichael (1991). Note that the small positive slope in (**B**) is the result of using values for $\overline{V}_{H_2O}^{melt}$ that do not vary with pressure, whereas the finite values of $\partial \overline{V}_{H_2O}^{melt}/\partial T$ and $\partial \overline{V}_{H_2O}^{melt}/\partial P$ result in increasing density of the anhydrous oxide components with increasing pressure. Filled symbols = melts on the join Na_2Si_4-O_9-$Na_2(NaAl)_4O_9$; open symbols = melts on the join K_2Si_4-O_9-$K_2(KAl)_4O_9$ (H_2O solubility data from Mysen and Acton 1999).

slightly negative (Kress and Carmichael 1991). The inverse correlation between density difference and Al_2O_3 content remains, even with fixed H_2O content, because of the negative correlation between $\overline{V}_{H_2O}^{melt}$ and Al_2O_3 of the melt.

The partial molar volume of H_2O dissolved in silicate melts most likely is not independent of pressure, in particular at low pressures (see also Fig. 9). This pressure effect diminishes, however, with increasing pressure and no effect of pressure on $\overline{V}_{H_2O}^{melt}$ can be discerned, within the error of the data, in the 0.8–2.0 GPa range for which volume properties were derived here (Figs. 7 and 8). For example, an exponential fit to the $\overline{V}_{H_2O}^{melt}$ extracted from the 1000 °C water-solubility isotherm for $NaAlSi_3O_8$ melt at $P \leq 0.5$ GPa (Hamilton and Oxtoby 1986) yields the expression:

$$\overline{V}_{H_2O}^{melt}\ (1000\ ^\circ C) = 10.62 + 38.49\ \exp[-0.0025 \cdot P\ (MPa)], \quad (3)$$

which indicates that $(\partial \overline{V}_{H_2O}^{melt}/\partial P)_T$ decreases exponentially with increasing pressure in this low-pressure range.

It is evident from Equation 3 that as pressure decreases, the density difference between hydrous and anhydrous melts may become quite significant. To evaluate this effect for felsic liquids, we chose composition NS4A6, which has NBO/T = 0.5 (anhydrous). This composition contains nearly 10 wt% Al_2O_3 (Table 1). In other words, composition NS4A6 may be considered a model andesite liquid.

To estimate the pressure dependence of $\overline{V}_{H_2O}^{melt}$ at $P < 0.8$ GPa, it was assumed that the 1000 °C pressure dependence of $\overline{V}_{H_2O}^{melt}$ for $NaAlSi_3O_8$ composition melt is the same as that of NS4A6 composition melt. The density difference between hydrous and anhydrous NS4A6 composition melts for 1, 3, and 5 wt% H_2O was then calculated at 1000 °C between 0.8 and 0.05 GPa (Fig. 11). The density difference between anhydrous and hydrous melt increases exponentially with decreasing total pressure so that at 200 MPa, for example, the density difference between anhydrous and hydrous haploandesitic magmatic liquid increases by 2–2.5% per wt% H_2O dissolved in the melt. In comparison, a 100 °C temperature increase of anhydrous NS4A6 melt at 200 MPa results in a density decrease of about 0.4–0.5%.

Water and density distribution in shallow magma chambers. Because melt density at upper crustal pressures is so sensitive to H_2O content, explosive volcanism associated with shallow dacite magma chambers may affect significantly the density distribution within the magma chamber itself.

The conditions surrounding the catastrophic eruption at Mount Pinatubo in June 1991 have been particularly well examined, and this system will be used as an example. At Mount Pinatubo in 1991, the temperature of the magma in the magma chamber was estimated to be near 800 °C (Rutherford and Devine 1996). This temperature is typical for other shallow, dacitic magma chambers (e.g., Foden 1986; Rutherford et al.

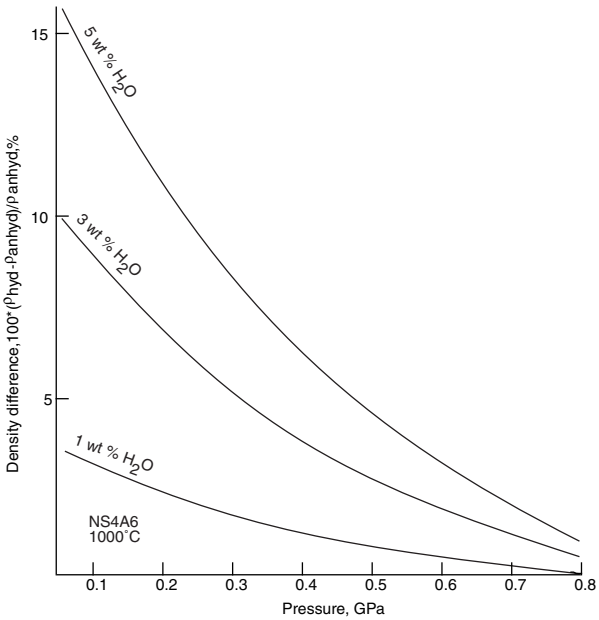

FIGURE 11. Density difference between hydrous, ρ_{hyd}, and anhydrous, ρ_{anhyd}, melts relative to that of anhydrous NS4A6 composition melt [$Na_2Si_4O_9$ + 6 mol% Al_2O_3 added as $Na_2(NaAl)_4O_9$ component] at 1000 °C over the range 0.05–0.8 GPa for the indicated water contents. Derivation of the partial molar volume, $\overline{V}^{melt}_{H_2O}$, used in this pressure range is discussed in the text.

1985; Mandeville et al. 1996). Prior to eruption, the pressure was ~0.22 GPa, the magma contained between 5.5 and 6.4 wt% water, and the melt was 30–50% crystallized (Rutherford and Devine 1996). The magma chambers associated with other, similar volcanic events (e.g., Bishop Tuff, Tambora 1815, Mount St. Helens) were also located at a depth corresponding to about 0.2 GPa at the onset of eruption. In those cases, the initial magmatic liquid also contained about 5–6 wt% H_2O (e.g., Skirius et al. 1990; Foden 1986; Rutherford et al. 1985). Thus, the magma chamber at Mount Pinatubo can be considered a typical example of shallow dacitic magma chambers associated with explosive volcanism.

The volume of the magma chamber at Mount Pinatubo in 1991 was between 40 and 125 km^3 (Wolfe and Hoblitt 1996; Mori et al. 1996). By using mid-range values for chamber size, crystallinity, and H_2O content (82.5 km^3, 40%, and 6 wt%), and a melt density of 2.3 g/cm^3 (Gerlach et al. 1996), the total H_2O content in the melt fraction in the chamber before the eruption is estimated to be $1.09 \cdot 10^{15}$ g. Gerlach et al. (1996) estimated that the total H_2O emission during this explosive event was $4.91 \cdot 10^{14}$ g H_2O.

The magma equivalent mass erupted during this event was 5–10 km^3. We will use a conservative estimate of 5 km^3 (Wolfe and Hoblit 1996). Some of the water loss can be ascribed to water exsolved from the extruded magma. Matrix glass from the 1991 Mount Pinatubo eruption contains ~0.3 wt% H_2O (Gerlach et al. 1996). If we assume 5 wt% H_2O in the magma at the time this material left the magma chamber, the difference between that water content and the amount of water found in the matrix glass converts to $\sim 1 \cdot 10^{14}$g for 5 km^3 of erupted magma. Consequently, ≥70% of the total H_2O emission must be water that originated from within the magma chamber itself. Thus, after the cataclysmic eruption in June 1991, the H_2O concentration in the remaining magma chamber (averaged over the entire chamber) was ~3.4 wt% H_2O.

With the NS4A6 melt composition model, if this volcanic activity occurred while the magma chamber remained at a constant temperature and pressure of 800 °C and 0.22 GPa, the average density of the magma remaining after the eruption would be 5.1% greater than the H_2O-saturated magma in the magma chamber before the eruption. By correcting for crystallinity (40%) and assuming no change in crystallinity during the several-day eruptive event, the magma (crystals+liquid) in the chamber after the eruption would have been about 3% more dense than before the eruptive event.

Some aspects of the conditions described above are, however, probably unrealistic for such magma chambers during and after explosive events. For example, once the initial explosion removed the material above the original magma chamber, the pressure near the top of the chamber probably was in the tens of MPa range owing to the thickness of the fragmentation front.[2] The H_2O-solubility in felsic magmatic liquids at 10 MPa, for example, is <1 wt% (Moore et al. 1998). The magma near the top of the magma chamber was, therefore, nearly anhydrous, consistent with H_2O analyses of extruded magma at Mount Pinatubo (Gerlach et al. 1996). The H_2O-solubility at 100 MPa (equivalent to the pressure near the bottom of a 2.7 km diameter spherical chamber) is about 4 wt% H_2O (Moore et al. 1998). If we assume no change in crystallinity (40%) in the magma chamber during the June 1991 eruptive event that lasted only for several days, our calculations indicate that the magma (crystals + liquid) at the top of the magma chamber was 0.07 g/cm^3, or about 3% more dense than the magma at the bottom of the chamber. In fact, by assuming that the residual magma was saturated with water along the pressure gradient from top to bottom, the density difference with depth, relative to that at the top of the chamber, would have been as shown in Figure 12. In other words, the residual magma in the chamber after an event such as that at Mount Pinatubo in June 1991 is gravitationally unstable. This density contrast might be compensated for by a thermal gradient down into the chamber. However, to neutralize the density difference by temperature alone, a thermal gradient near 250 °C/km is required, which is a wholly unrealistic value. Thus, in a magma chamber of fixed bulk composition similar to that modeled by the haploandesite composition

[2]If we use the relationship between pressure drop in a magma chamber, ΔP, and volume of extruded magma, ΔV (e.g., Druitt and Sparks 1984), from the ΔV values given by Daag et al. (1996), the pressure drop, ΔP, would be 200–300 MPa assuming the bulk modulus of hydrous andesite magma is 20–30 GPa. In other words, from this estimate, the top of the magma chamber after the eruption would be at nearly ambient pressure conditions.

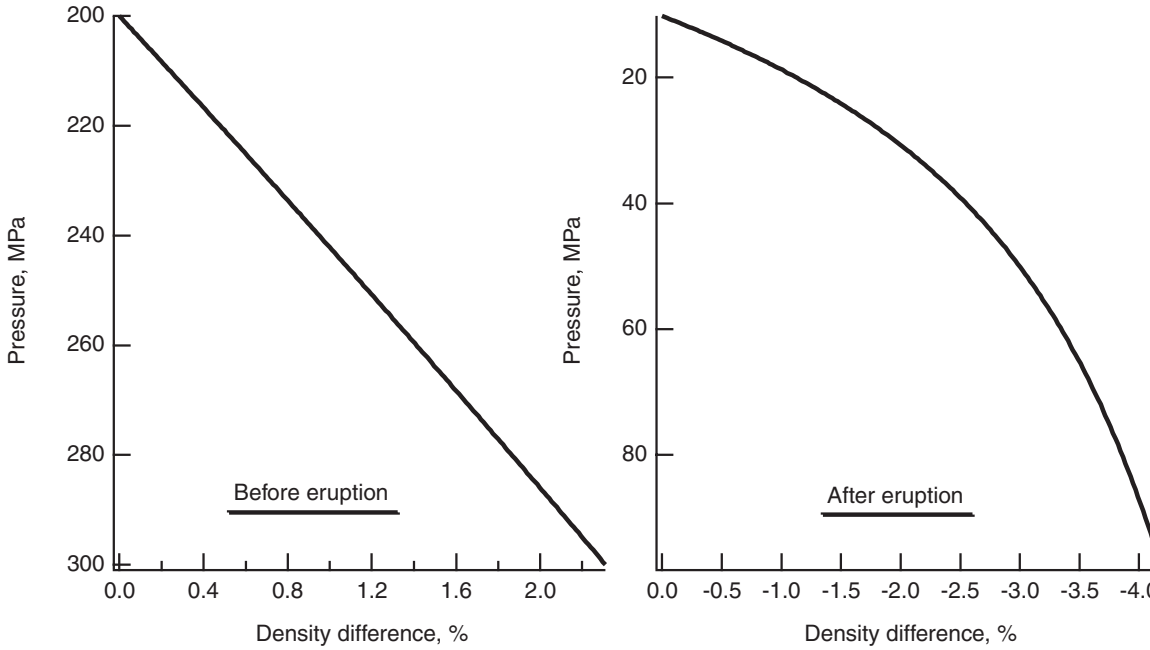

FIGURE 12. Density difference, $100(\rho_{hyd}-\rho_{anhyd})/\rho_{anhyd}$, trend in shallow felsic magma chambers such as that associated with the June 1991 explosive eruption at Mount Pinatubo, Philippines, calculated for 800 °C. The parameters needed for this calculation (chamber size, crystallinity, temperature, and initial H_2O content) are discussed in the text. The conditions before the eruption are expressed in terms of pressure with an overburden above the magma chamber equivalent to 200 MPa pressure. Water concentration, bulk composition, and crystallinity throughout the magma chamber are assumed not to vary (see text for details). It is further assumed that after the eruption, the pressure at the top of the chamber was 10 MPa due to the weight of the overlying fragmented rock. Lower pressure results in greater density contrasts in the chamber. It is assumed that the residual magma in the chamber was water-saturated (solubility calculated from the equation given by Moore et al. 1998), and that temperature and crystallinity did not change during the several-day period of this eruptive event.

NS4A6, convective overturn within the chamber following such catastrophic eruptive events is possible.

Plinian events such as the eruption of Mount St. Helens in 1980 or Tambora in 1815 were qualitatively similar. It is likely, therefore, that in any catastrophic eruption associated with a shallow (~5–10 km deep) dacitic magma chamber, the density of the magma in the chamber after the eruption would be significantly greater than prior to the event. Further, the uppermost portions of any residual magma in the magma chamber after an explosive eruption would be more dense than the magma in the lower part of the chamber.

ACKNOWLEDGMENTS

This research was conducted with partial support from NSF grants EAR-9901886 and REU-9619551. Critical reviews by R. Lange and two anonymous reviewers greatly improved and clarified this manuscript. Able laboratory assistance by Lora Armstrong greatly simplified the data acquisition.

REFERENCES CITED

Boyd, F.R. and England, J.L. (1960) Apparatus for phase equilibrium measurements at pressures up to 50 kilobars and temperatures up to 1750°C. Journal of Geophysical Research, 65, 741–748.

Brodholt, J. and Wood, B.J. (1993) Simulations of the structure and thermodynamic properties of water at high pressures and temperatures. Journal of Geophysical Research, 98, 519–536.

Bureau, H. and Keppler, H. (1999) Complete miscibility between silicate melts and hydrous fluids in the upper mantle; experimental evidence and geochemical implications. Earth and Planetary Science Letters, 165, 187–196.

Burnham, C.W. and Davis, N.F. (1971) The role of H_2O in silicate melts. I. P-V-T relations in the system $NaAlSi_3O_8$-H_2O to 10 kilobars and 1000°C. American Journal of Science, 270, 54–79.

Burnham, C.W. and Jahns, R.H. (1962) A method for determining the solubility of water in silicate melts. American Journal of Science, 261, 721–745.

Clemens, J.D. and Navrotsky, A. (1987) Mixing properties of $NaAlSi_3O_8$-H_2O melts; new calorimetric data and some geological implications. Journal of Geology, 95, 173–186.

Daag, A.S., Dolan, M.T., Laguerta, E.P., Meeker, G.P., Newhall, G.C., Pallister, J.S., and Solidum, R.U. (1996) Growth of a post-climatic dome at Mount Pinatubo, July-October 1992. In C.G. Newhall, and R.S. Punongbayan, Eds. Fire and Mud; Eruptions and lahars of Mount Pinatubo, Philippines., p. 647–664. Philippine Institute of Volcanology and Seismology, Quezon City, Philippines and University of Washington Press, U.S.

Dingwell, D.B., Holtz, F., and Behrens, H. (1997) The solubility of H_2O in peralkaline and peraluminous granitic melts. American Mineralogist, 82, 434–437.

Dingwell, D.B., Hess, K.-U., and Romano, C. (1998) Viscosity data for hydrous peraluminous granitic melts: Comparison with the metaluminous model. American Mineralogist, 83, 236–239.

Druitt, T.H. and Sparks, R.S.J. (1984) On the formation of calderas during ignimbrite eruptions. Nature (London), 310, 679–681.

Foden, J. (1986) The petrology of the Tambora volcano, Indonesia; a model for the 1815 eruption. Journal of Volcanology and Geothermal Research, 27, 1–41.

Gaetani, G.A., Grove, T.L., and Bryan, W.B. (1993) The influence of water on the petrogenesis of subduction-related igneous rocks. Nature, 365, 332–334.

Gerlach, T.M., Westrich, H.R., and Symonds, R.B. (1996) Pre-eruption vapor in magma of the climactic Mount Pinatubo eruption: Source of the giant stratospheric sulfur dioxide cloud. In C.G. Newhall, and R.S. Punongbayan, Eds., Fire and Mud; Eruptions and lahars of Mount Pinatubo, Philippines., p. 415–434. Philippine Institute of Volcanology and Seismology, Quezon City, Philippines and University of Washington Press, U.S.

Haar, L., Gallagher, J.S., and Kell, G.S. (1984) Steam Tables. Thermodynamic and transport properties and computer programs for vapor and liquid states of water

in SI units. 320 p. Hemisphere Publishing Corporation, New York.
Hamilton, D.L. and Oxtoby, S. (1986) Solubility of water in albite melt determined by the weight loss method. Journal of Geology, 94, 616–630.
Hodges, F.N. (1974) The solubility of H_2O in silicate melts. Carnegie Institution of Washington Year Book, 73, 251–255.
Holtz, F., Behrens, H., Dingwell, D.B., and Johannes, W. (1995) H_2O solubility in haplogranitic melts: Compositional, pressure, and temperature dependence. American Mineralogist, 80, 94–108.
Kohn, S.C., Dupree, R., and Mortuza, M.G. (1992) The interaction between water and aluminosilicate magmas. In Y. Bottinga, D.B. Dingwell, and P. Richet, Eds., Silicate melts, 96, p. 399–409. Elsevier, Amsterdam, Netherlands.
Kress, V.C. and Carmichael, I.S.E. (1991) The compressibility of silicate liquids containing Fe_2O_3 and the effect of composition, temperature, oxygen fugacity and pressure on their redox states. Contributions to Mineralogy and Petrology, 108, 92–92.
Kushiro, I. (1972) Effect of water on the composition of magmas formed at high pressures. Journal of Petrology, 13, 311–334.
———(1976) A new furnace assembly with a small temperature gradient in solid-media, high-pressure apparatus. Carnegie Institution of Washington Year Book, 75, 832–833.
———(1978) Density and viscosity of hydrous calc-alkalic andesite magma at high pressure. Carnegie Instn. Washington Year Book, 77, 675–678.
———(1990) Partial melting of mantle wedge and evolution of island arc crust. Journal of Geophysical Research, 95, 15,929–15,939.
Lange, R.A. (1994) The effect of H_2O, CO_2, and F on the density and viscosity of silicate melts. In M.R. Carroll, and J.R. Holloway, Eds. Volatiles in Magmas, p. 331–370. Mineralogical Society of America, Washington, D.C.
Lange, R.A. and Carmichael, I.S.E. (1987) Densities of Na_2O-K_2O-CaO-MgO-Fe_2O_3-Al_2O_3-TiO_2-SiO_2 liquids: New-measurements and derived partial molar properties. Geochimica et Cosmochimica Acta, 51, 2931–2946.
Mandeville, C.W., Carey, S., and Sigurdsson, H. (1996) Magma mixing, fractional crystallization and volatile degassing during the 1883 eruption of Krakatau Volcano, Indonesia. Journal of Volcanology and Geothermal Research, 74(3–4), 243–274.
Moore, G., Vennemann, T., and Carmichael, I.S.E. (1998) An empirical model for the solubility of H_2O in magmas to 3 kilobars. American Mineralogist, 83, 36–42.
Mori, J., Eberhart-Phillips, D., and Harlow, D.H. (1996) Three-dimensional velocity structure at Mount Pinatubo: Resolving magma bodies and earthquake hypocenters. In C.G. Newhall and R.S. Punongbayan, Eds., Fire and Mud; Eruptions and lahars of Mount Pinatubo, Philippines., p. 371–381. Philippine Institute of Volcanology and Seismology, Quezon City, Philippines and University of Washington Press, U.S.
Mysen, B.O. (1990) Relationships between melt structure and petrologic processes. Earth-Sciience Review, 27, 261–365.
Mysen, B.O. and Acton, M. (1999) Water in H_2O-saturated magma-fluid systems: Solubility behavior in K_2O-Al_2O_3-SiO_2-H_2O to 2.0 GPa and 1300°C. Geochimica et Cosmochimica Acta, 63, 3799–3815.
Mysen, B.O. and Boettcher, A.L. (1975) Melting of a hydrous mantle. II. Geochemistry of crystals and liquids formed by anatexis of mantle peridotite at high pressures and high temperatures as a function of controlled activities of water, hydrogen and carbon dioxide. Journal of Petrology 16, 549–590.
Mysen, B.O. and Virgo, D. (1986) The structure of melts in the system Na_2O-CaO-Al_2O_3-SiO_2-H_2O quenched from high temperature at high pressure. Chemical Geology, 57, 333–358.
Nowak, M. and Behrens, H. (1995) The speciation of water in haplogranitic glasses and melts by in-situ, near-infrared spectroscopy. Geochimica et Cosmochimica Acta, 59, 3445–3450.
———(1997) An experimental investigation on diffusion of water in haplogranitic melts. Contributions to Mieralogy and Petrology, 126, 365–376.
Ochs, F.A. and Lange, R.A. (1997) The partial molar volume, thermal expansivity, and compressibility of H_2O in $NaAlSi_3O_8$ liquid: new measurements and an internally consistent mode. Contributions to Mineralogy and Petrology, 129, 155–165.
Paillat, O., Elphick, E.C., and Brown, W.L. (1992) The solubility behavior of H_2O in $NaAlSi_3O_8$ melts: A re-examination of Ab-H_2O phase relationships and critical behavior at high pressure. Contributions to Mieralogy and Petrology, 112, 490–500.
Richet, P. and Polian, A. (1998) Water as a dense icelike component in silicate glasses. Science, 281(5375), 396–398.
Rutherford, M.J. and Devine, J.D. (1996) Pre-eruption pressure-temperature conditions and volatiles in the 1991 dacitic magma of Mount Pinatubo. In C.G. Newhall, and R.S. Punongbayan, Eds., Fire and Mud; Eruptions and lahars of Mount Pinatubo, Philippines., p. 751–766. Philippine Institute of Volcanology and Seismology, Quezon City, Philippines and University of Washington Press, U.S.
Rutherford, M.J., Sigurdsson, H., Carey, S., and Davis, A. (1985) The May 18, 1980, eruption of Mount St. Helens; 1, Melt composition and experimental phase equilibria. Journal of Geophysical Research. B, 90, 2929–2947.
Schulze, F., Behrens, H., Holtz, F., Roux, J., and Johannes, W. (1996) The influence of H_2O on the viscosity of haplogranitic melt. American Mineralogist, 81, 1155–1165.
Shen, A. and Keppler, H. (1995) Infrared spectroscopy of hydrous silicate melts to 1000°C and 10 kbar: Direct observation of H_2O speciation in a diamond cell. American Mineralogist, 80, 1335–1338.
Shen, A.H. and Keppler, H. (1997) Direct observation of complete miscibility in the albite-H_2O system. Nature, 385, 710–712.
Skirius, C.M., Peterson, J.W., and Anderson, A.T. (1990) Homogenizing rhyolitic glass inclusions from the Bishop Tuff. American Mineralogist, 75, 1381–1398.
Stalder, R., Ulmer, P., Thompson, A.B., and Gunther, D. (2000) Experimental approach to constrain second critical endpoints in fluid/silicate systems: Near-solidus fluids and melts in the system abite-H_2O. American Mineralogist, 85, 68–77.
Stolper, E. (1982) The speciation of water in silicate melts. Geochimica et Cosmochimica Acta, 46, 2609–2620.
Withers, A.C., Zhang, Y., and Behrens, H. (1999) Reconciliation of experimental results on H_2O speciation innrhyolitic glass using in-situ and quenchinh techniques. Earth and Planetary Science Letters 173, 343–349.
Wolfe, E.W. and Hoblitt, R.P. (1996) Overview of the eruptions. In C.G. Newhall, and R.S. Punongbayan, Eds. Fire and Mud; Eruptions and lahars of Mount Pinatubo, Philippines., p. 3–21. Philippine Institute of Volcanology and Seismology, Quezon City, Philippines and University of Washington Press, U.S.
Zhang, Y. and Stolper, E.M. (1991) Water diffusion in a basaltic melt. Nature, 351, 306–309.

MANUSCRIPT RECEIVED OCTOBER 19, 1999
MANUSCRIPT ACCEPTED APRIL 20, 2000
PAPER HANDLED BY ROBERT F. DYMEK